applied sciences

MDPI

Article

Study on Interior Aerodynamic Noise Characteristics of the High-Speed Maglev Train in the Low Vacuum Tube

Jiali Liu [1], Mengge Yu [2,*], Dawei Chen [1] and Zhigang Yang [3]

[1] CRRC Qingdao Sifang Co., Ltd., Qingdao 266111, China
[2] College of Mechanical and Electrical Engineering, Qingdao University, Qingdao 266071, China
[3] Key Laboratory of Traffic Safety on Track, Ministry of Education, School of Traffic & Transportation Engineering, Central South University, Changsha 410075, China
* Correspondence: yumengge0627@163.com; Tel.: +86-532-6895-3590

Abstract: As the next-generation high-speed transportation system, the low vacuum tube high-speed maglev system combines the tube with a certain degree of vacuum with the high-speed maglev train, which can realize high-speed operation under low aerodynamic resistance and noise mode. In order to study the interior aerodynamic noise characteristics of the high-speed maglev train in the low vacuum tube, a computational model of the external flow field of the high-speed maglev train in a low vacuum tube was established, and the computational model of the interior aerodynamic noise of the high-speed maglev train was established using the statistical energy analysis method; then the interior aerodynamic noise characteristics of the high-speed maglev train in the low vacuum tube were studied. The research results show that in the low vacuum tube, the distribution of the interior aerodynamic noise of the high-speed maglev train shows the characteristics of large head car and tail car and small middle car, and the aerodynamic noise on the top of the car is smaller than that on the floor. With the increase in frequency, the sound pressure level of the interior aerodynamic noise of the high-speed maglev train has the tendency of increasing first and then decreasing, and the main energy of the interior aerodynamic noise is distributed in the range of 200–1000 Hz. From the perspective of the total sound pressure level of the interior aerodynamic noise, the interior aerodynamic noise of the tail car is the greatest, followed by the head car, and the interior aerodynamic noise of the middle car is the smallest. As the direction of the travel of the maglev train will change, the optimization design of the interior aerodynamic noise of the head and tail cars should be emphasized.

Keywords: high-speed maglev train; low vacuum tube; interior aerodynamic noise; statistical energy analysis

Citation: Liu, J.; Yu, M.; Chen, D.; Yang, Z. Study on Interior Aerodynamic Noise Characteristics of the High-Speed Maglev Train in the Low Vacuum Tube. *Appl. Sci.* **2022**, *12*, 11444. https://doi.org/10.3390/app122211444

Academic Editor: Alberto Corigliano

Received: 13 September 2022
Accepted: 2 November 2022
Published: 11 November 2022

1. Introduction

In recent years, China's high-speed railway has achieved rapid development, the operational speed of the train has also been continuously improved. Train aerodynamic problems have become very significant [1–4]. The aerodynamic drag force is approximately square with the train speed, and the aerodynamic noise is proportional to the 6–8th power of the train speed [5,6]. There are the objective laws that cannot be avoided by any form of ground transportation. To obtain the higher running speed near the ground, the fundamental way can only be to change the density of the medium. The cruising altitude of mainline aircraft reaches 10,000 m, which can remove the dense atmosphere. The ground train cannot fly to an altitude of 10,000 m. However, the closed tube can be used to reduce the density of the air, which is equivalent to creating a low-density medium environment around the ground train. Therefore, the ground train can be freed of the constraints of the aerodynamic drag force and aerodynamic noise, and in theory, can achieve higher running speed. The low vacuum tube high-speed maglev system combines a tube with a certain degree of vacuum and the high-speed maglev train, which can realize high-speed operation

with low aerodynamic drag force and aerodynamic noise. In 1999, Oster and Fla received the patent for the invention of the vacuum tube transportation system. In 2013, Elon Musk proposed the plan for the Hyperloop. In China, in 2004, the academician's academic report "Vacuum Tube High-speed Transportation", jointly initiated by Shen Zhiyun and Zhong Shan, was successfully held at the Southwest Jiaotong University, to discuss the scientific nature, reality, development prospect and great significance of the vacuum tube high-speed transportation system. In 2014, the world's first vacuum tube high-temperature superconducting maglev train experimental platform "Super-Maglev", which integrated traction, communication and pressure testing, was established in the State Key Laboratory of Traction Power of Southwest Jiaotong University [7,8].

There has been an upsurge in research regarding vacuum tube high-speed maglev trains in the world. The research on the aerodynamics of the high-speed maglev train in the low vacuum tube is in its infancy, and the related research work is little. Kim T.K. used the two-dimensional compressible model to study the relationship between the aerodynamic drag force of the high-speed train in the vacuum tube and train speed, blocking ratio, and tube pressure [9]. Oh J.S. studied the influence of the blockage ratio, pod speed, pod length, tube pressure, and temperature on the aerodynamic drag force of the Hyperloop system, and found that the pressure drag force is significantly affected as the blockage ratio increased; strong shock waves occurred near the end of the pod as the pod speed increased [10]. Braun J. and Opegenoord M.M.J. performed the aerodynamic shape design and optimization of the Hyperloop train body to ensure a certain aerodynamic lift force of the car body and reduce the aerodynamic drag force [11,12]. Niu J.Q. and Zhou P. used two-dimensional dynamic grid technology to study the development of shock waves and the aerothermal effects inside the vacuum tube under unsteady conditions [13–16]. Yang Y. established the parametric shape of the vacuum tube train, and took the aerodynamic drag force as the optimization objective. After the optimization, the aerodynamic drag force of the train was reduced by 5.52% [17]. Zhang X.H. studied the influence of the length of the streamlined head on the aerodynamic drag force of the train in the vacuum tube [18]. Nick N. used the numerical simulation method to study the aerodynamic flow separation position of the vacuum duct aircraft, and optimized the aerodynamic shape of the aircraft [19]. The existing research work mainly focuses on the aerodynamic characteristics of the train in the low vacuum tube, and rarely involves the problem of the aerodynamic noise. In the vacuum tube, the external aerodynamic noise of the high-speed maglev train will not affect the environment, but will affect the interior noise of the train. The interior aerodynamic noise of the high-speed maglev train in the vacuum tube will affect the comfort of the passengers. Klühspies J. conducted an international survey on "Hyperloop" in the transport sector, and found that the importance of low noise levels was also evident from the information provided by survey respondents. For example, of 93% (588 responses) of survey respondents, 54.3% (343) rated a low noise level in the interior as 'extremely important' and 38.8% (245) rated it as 'rather important' for a one-hour Hyperloop trip. Only 7% (44) of survey participants rated noise emissions in the vehicle as 'Unimportant' or 'Rather unimportant' [20]. Therefore, the interior aerodynamic noise characteristics of the high-speed maglev train in the vacuum tube will be studied in the present paper. In Section 2, the computational model of the external flow field of the high-speed maglev train in the low vacuum tube is established by the large eddy simulation method. In Section 3, the computational model of the interior aerodynamic noise of the high-speed maglev train is established using the statistical energy analysis method. In Section 4, the interior aerodynamic noise characteristics of the high-speed maglev train in the vacuum tube are studied.

2. Computational Model of External Flow Field

2.1. Fluid Model

To carry out the computation for under low vacuum environment, the suitability of the continuum model should be considered. In the tube, as the tube pressure decreases,

the density of the air in the tube decreases, that is, the air in the tube becomes thinner. The Knudsen number (denoted as Kn) is usually used to indicate the thinness of the air. The air flow can be divided into three areas according to the thinness of the air, namely, the slip field ($0.01 < Kn < 0.1$), the transition field ($0.1 < Kn < 10$), and the free molecular flow field ($Kn > 10$). When $Kn < 0.01$, the air flow can be considered to be in the continuous domain, in which the continuum model can be used to describe the air flow.

The Knudsen number, Kn, is defined as the ratio of the average free path of the molecule to the characteristic length of the flow, and its expression is:

$$Kn = \frac{\lambda}{L} \tag{1}$$

where λ is the average free path of the molecule and L is the characteristic length of the flow.

The average free path of the molecule can be expressed as:

$$\lambda = \frac{k_B T}{\sqrt{2}\pi d^2 p} \tag{2}$$

where k_B is the Boltzmann constant, $k_B = 1.3805 \times 10^{-23}$; T is the temperature; d is the molecular diameter; and p is the pressure.

When the temperature is 298 K, the average free path of the molecule under the standard atmospheric pressure is $\lambda = 6.11 \times 10^{-8}$ m. In the present paper, the tube pressure in the low vacuum tube is 0.3 atm, and the corresponding average free path of the molecule is $\lambda = 1.02 \times 10^{-7}$ m. The height of the high-speed train can be taken as the characteristic length of the flow, which is usually about 4.0 m. Therefore, in the present paper, the Knudsen number is:

$$Kn = 2.55 \times 10^{-8} << 0.01 \tag{3}$$

The air flow in the low vacuum tube in the present paper is in the continuous field, and the continuous medium model can be used to describe the air flow characteristics in the low vacuum tube.

2.2. Governing Equations

Compressibility is a basic property of a fluid. Any fluid is compressible, but when the influence of the change of fluid density on the flow can be ignored, the incompressible flow assumption can be adopted, that is, the density is constant. Usually, the train speed does not exceed 350 km/h (the corresponding Mach number is 0.286), and the influence of the change of air density on the flow is negligible and incompressible flow can be used. However, in the present paper, the speed of the high-speed maglev train is 600 km/h, and the corresponding Mach number is 0.49, which is significantly higher than 0.3. The compressibility of the air should be considered. In addition, the low vacuum tube is a closed structure, and the compressibility of the air should also be considered. Therefore, the flow field of the high-speed maglev train in the low vacuum tube can be described by the three-dimensional compressible Navier–Stokes equation.

The flow field around the high-speed maglev train is a very complex turbulent flow field. It is necessary to simulate the turbulent flow to obtain the flow field of the high-speed maglev train. In order to study the characteristics of the aerodynamic noise source of the high-speed maglev train, the fluctuating characteristics of the surface pressure of the high-speed maglev train should be accurately computed; therefore, the large eddy simulation (LES) method is used to simulate the turbulent flow field of the high-speed maglev train [21,22].

The basic idea of the LES is to decompose the instantaneous turbulent flow including fluctuating motion into two parts, namely, large-scale eddy motion and small-scale eddy motion, through a certain filtering method. The large-scale vortex motion can be obtained by directly solving the Navier–Stokes equation, and the influence of the small-scale vortex motion on the large-scale vortex motion is expressed in the motion equation as a stress

term similar to the Reynolds stress, which is called sub-grid Reynolds stress. Sub-grid Reynolds stress can be simulated by establishing the model. After filtering the Navier–Stokes equation, the governing equations of the LES can be obtained as:

$$\frac{\partial \rho}{\partial t} + \frac{\partial (\rho \overline{u}_j)}{\partial x_j} = 0 \tag{4}$$

$$\frac{\partial (\rho \overline{u}_i)}{\partial t} + \frac{\partial (\rho \overline{u}_i \overline{u}_j)}{\partial x_j} = -\frac{\partial \overline{p}}{\partial x_i} + \frac{\partial \overline{\tau}_{ij}}{\partial x_j} - \frac{\partial \tau_{ij}^l}{\partial x_j} \tag{5}$$

where $\overline{u}_i$ is the velocity component after spatial filtering, $\overline{\tau}_{ij}$ is the viscous stress tensor after spatial filtering, and τ_{ij}^l is the sub-grid Reynolds stress.

In order to close the equations, it is necessary to model the sub-grid Reynolds stress. The commonly used model is the eddy viscosity model:

$$\tau_{ij}^l - \frac{1}{3}\overline{\tau}_{kk}\delta_{ij} = -2\mu_i \overline{S}_{ij} \tag{6}$$

where μ_i is the sub-grid viscosity coefficient and $\overline{S}_{ij}$ is the sub-grid tensor rotation rate, which can be expressed as:

$$\overline{S}_{ij} = \frac{1}{2}\left(\frac{\partial \overline{u}_i}{\partial x_j} + \frac{\partial \overline{u}_j}{\partial x_i}\right) \tag{7}$$

The Smagorinsky–Lilly model is commonly used to compute the sub-grid viscosity coefficient. In this model, the sub-grid viscosity coefficient can be expressed as:

$$\mu_t = \rho L_s \sqrt{2\overline{S}_{ij}\overline{S}_{ij}} \tag{8}$$

where L_s is the sub-grid mixing length, and can be computed by

$$L_s = \min\left(\kappa d, C_s V^{1/3}\right) \tag{9}$$

where C_s is the Smagorinsky constant, κ is the von Karman constant, d is the distance to the nearest wall, and V is the volume of the computation cell. C_s is 0.1 in the Smagorinsky–Lilly model.

2.3. Numerical Model

Figure 1 shows the geometric model of the high-speed maglev train. The maglev train is a five-car marshalling model with a scale of 1:8. Figure 2 shows the computational domain. The cross section of the low vacuum tube is fan-shaped with an area of 80 m^2. In order to ensure the stability of the computation in the low vacuum tube (that is, to suppress the numerical oscillation in the vacuum tube), in the longitudinal direction, the distance from the front end of the maglev train to the entrance boundary is 200 m, and the distance from the rear end of the maglev train to the exit boundary is 500 m. In the transverse direction, the entire computational domain is symmetric along the longitudinal symmetry plane of the maglev train. The front inlet of the computational domain is set as the pressure far field (given incoming flow Mach number) and non-reflective boundary conditions, the back end of the computational domain is set as the pressure outlet and non-reflective boundary conditions, the track and low vacuum tube are set as the sliding walls boundary conditions, the speed is consistent with the incoming flow speed, and the high-speed maglev train is set as the fixed wall.

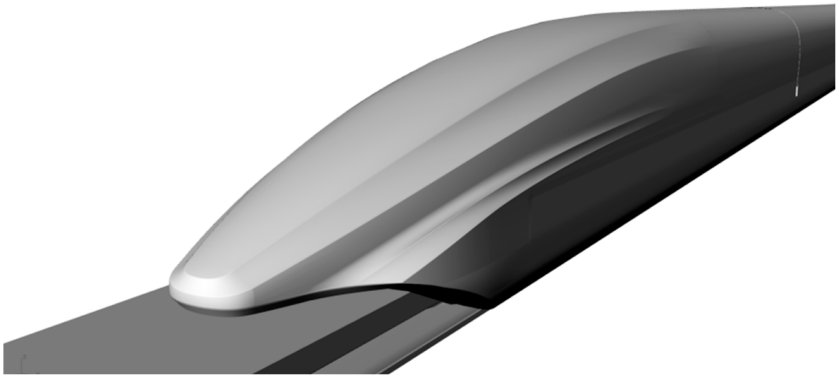

Figure 1. High-speed maglev model.

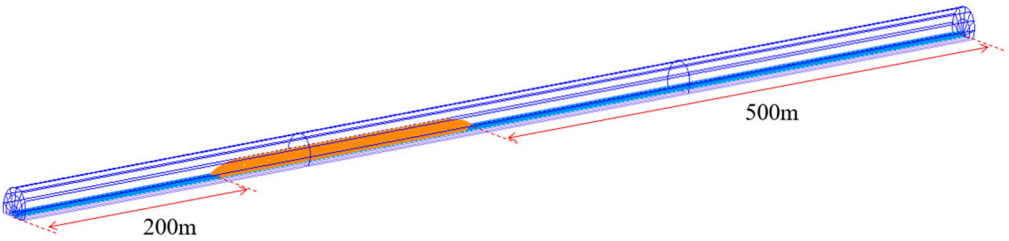

Figure 2. Computational model.

Commercial software, ICEM, is used for meshing, and the refined tetrahedral/triangular prism meshing is carried out through topology optimization, multi-layer mesh encryption technology, boundary layer mesh technology, and mesh stretching technology. The maximum mesh size of the streamlined parts of the head and tail cars is 30 mm, the maximum mesh size of the body parts of the head and tail cars is 40 mm, and the maximum mesh size of the middle car is 60 mm. Three encryption zones are set up around the high-speed maglev train. The maximum sizes of the encryption zone are 20 mm, 40 mm, and 60 mm, respectively. The streamlined part of the tail car is individually encrypted, and the maximum mesh size is 10 mm. The boundary layer mesh is set on the surface of the high-speed maglev train. The number of boundary layers is 8, and the total thickness is 0.3 mm. The number of computational meshes is more than 100 million. Figure 3 shows the computational mesh.

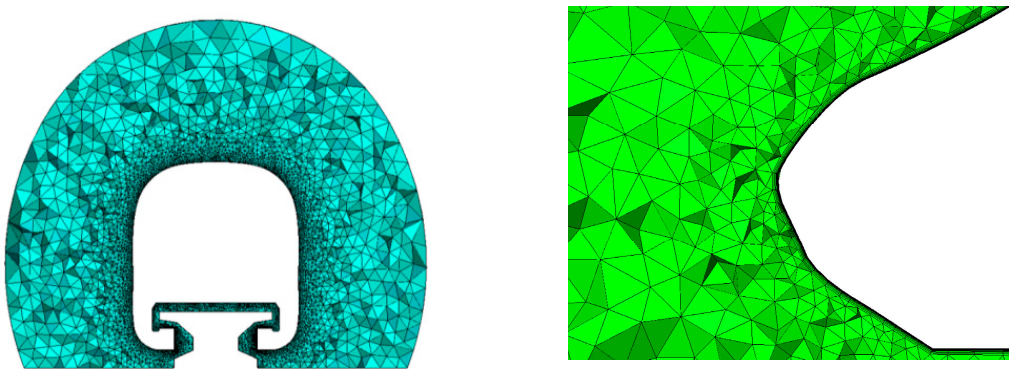

(**a**) (**b**)

Figure 3. Computational mesh: (**a**) Cross-section mesh, (**b**) boundary layer mesh.

The steady flow field is computed firstly, then the unsteady flow field is computed. For steady computation, the SST k-ω turbulence model is adopted for the turbulence simulation, the semi-implicit method for pressure-linked equations (SIMPLE) algorithm

is adopted for solving the pressure–velocity coupling, the standard scheme is used for discretizing the pressure equation, and the second upwind scheme is used for discretizing the momentum equation, turbulent kinetic energy equation, and turbulent dissipation equation. For unsteadiness computation, the steady flow field is set as the initial flow field, the LES method is adopted for the turbulent simulation, and the sub-grid model is the Smagorinsky model. The coupled algorithm is adopted for solving the pressure–velocity coupling. The unsteady calculation time step is 5×10^{-5} s, and a total of 10,000 time-steps are computed. Figure 4 shows the y^+ on the train surface. As shown in Figure 4, the y^+ on the majority of the train surface region is less than 1, which could meet the computational requirement of the LES method.

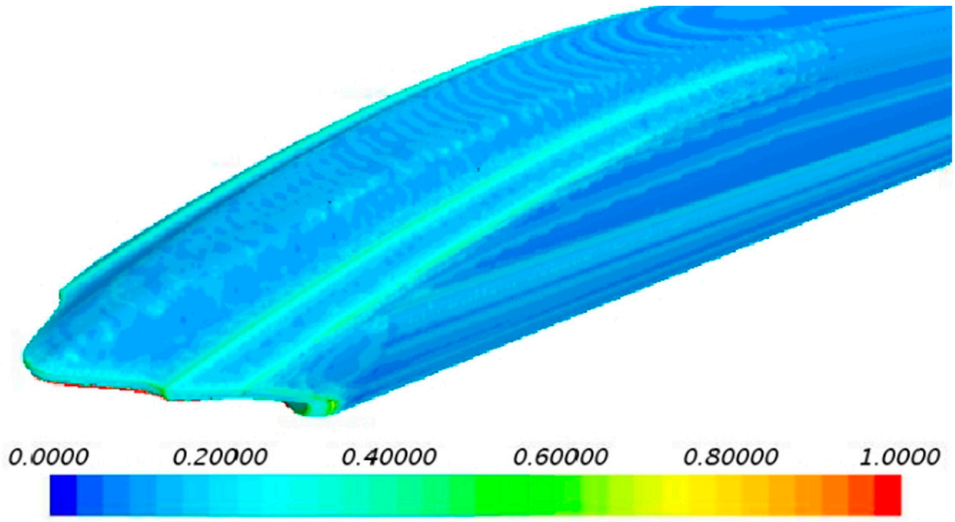

Figure 4. The y^+ on the train surface.

The computational model is verified by comparing the computational results of the pressure on the train surface with the wind tunnel test results. The wind tunnel test model is a three-car marshalling model with a scale of 1:8. The computational model for the model verification is consistent with the wind tunnel test model, and the mesh division method and the computational setting are consistent with those in Section 2.3. Figure 5 shows the comparison between the computational results of the pressure coefficient on the longitudinal symmetry line of the train and the wind tunnel test results. As shown in Figure 5, the computational results of the pressure coefficient on the longitudinal symmetry line of the head and tail cars are in good agreement with the wind tunnel test results, thus the mesh division method and computational settings in the present paper are reliable.

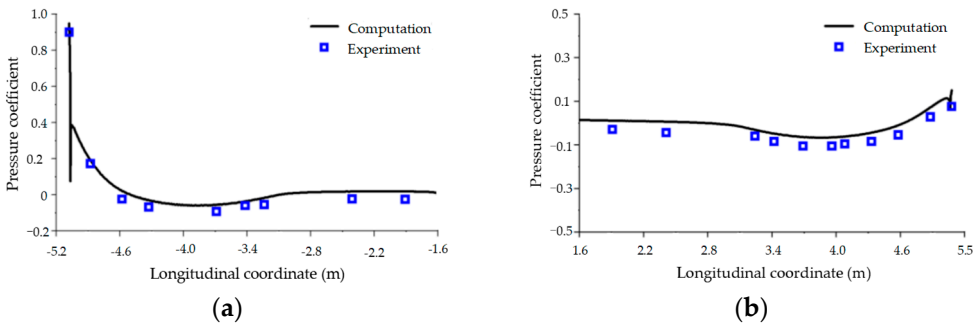

Figure 5. Comparison of the pressure coefficient: (**a**) Head car, (**b**) tail car.

3. Computational Model of Interior Aerodynamic Noise

3.1. Statistical Energy Analysis Model

When the high-speed maglev train is running, a huge fluctuating pressure is generated on the train surface, which in turn generates a large amount of aerodynamic noise inside the maglev train. The fluctuating pressure on the train surface has high and wide frequency characteristics, and the structure of the train body is very complex. Thus, the dynamic response of the body panels, windows, door, etc. caused by the fluctuating pressure on the train surface is very complex. The statistical energy analysis is a statistical method for analyzing random noise in a wide frequency range. It analyzes the transfer level of the average vibration energy of dense modes from a statistical point of view. This method is suitable for complex systems with high frequency and high modal density, which can effectively predict the dynamic response of the complex engineering structural systems under the high frequency broadband random excitation [23,24].

Statistical energy analysis is mainly based on the statistics of modal density, internal loss factor, and coupling loss factor of each subsystem, and calculates the vibration energy transmission between subsystems in the form of power flow. The core of statistical energy analysis is the power flow balance equation. Assuming that the main energy flow between subsystems is caused by structural resonance or acoustic mode, when the vibration power flows from one subsystem to another linked subsystem, the power loss and flow law are shown in Figure 6.

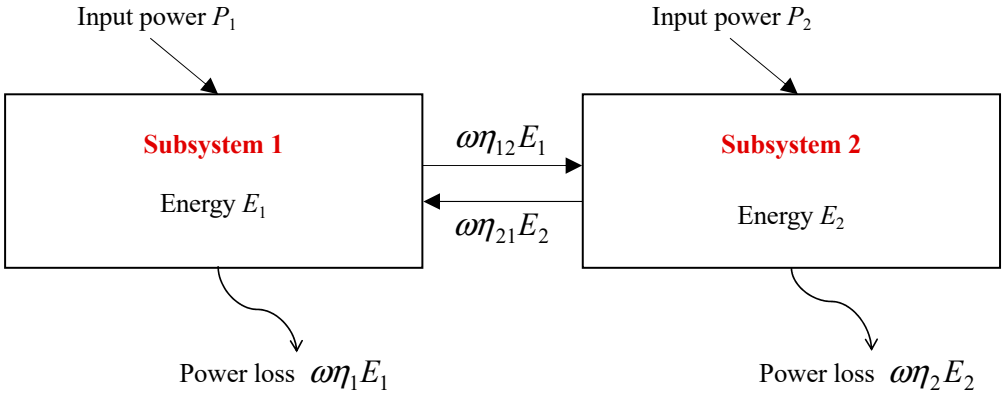

Figure 6. Statistical energy analysis model of two subsystems.

Generally, the subsystem is defined as a finite area with the same resonant modal performance, and the average modal energy depends on the balance between the external input energy, energy loss, and energy exchange. Therefore, the power balance equations between two subsystems are:

$$P_1 = \omega\eta_1 E_1 + \omega\eta_{12} n_1 \left(\frac{E_1}{n_1} - \frac{E_2}{n_2} \right) \tag{10}$$

$$P_2 = \omega\eta_2 E_2 + \omega\eta_{21} n_2 \left(\frac{E_2}{n_2} - \frac{E_1}{n_1} \right) \tag{11}$$

If the system has m subsystems, the m power balance equation will be generated, written in matrix form as:

$$\omega \begin{bmatrix} \eta_{11}n_1 & -\eta_{12}n_1 & \cdots & -\eta_{1m}n_1 \\ -\eta_{21}n_2 & \eta_{22}n_2 & \cdots & -\eta_{2m}n_1 \\ \vdots & \vdots & \ddots & \vdots \\ -\eta_{m1}n_2 & -\eta_{m2}n_2 & \cdots & \eta_{mm}n_m \end{bmatrix} \begin{bmatrix} E_1/n_1 \\ E_2/n_2 \\ \vdots \\ E_m/n_m \end{bmatrix} = \begin{bmatrix} P_1 \\ P_2 \\ \vdots \\ P_m \end{bmatrix} \tag{12}$$

$$\eta_{ii} = \eta_i + \sum_{j=1, j\neq i}^{m} \eta_{ij} \tag{13}$$

where ω is the center frequency within the bandwidth, P_i is the external input power of subsystem i, η_{ij} is the coupling loss factor from subsystem i and from subsystem j, η_i is the internal loss factor of subsystem i, n_i is the modal density of subsystem i, and E_i is the energy of subsystem i.

For the conservation coupling system, the transmission power between the coupling systems meets the reciprocity principle, thus there are:

$$n_i \eta_{ij} = n_j \eta_{ji} \tag{14}$$

Then, the power flow balance equation can be rewritten as:

$$\omega \begin{bmatrix} \eta_{11} & -\eta_{21} & \cdots & -\eta_{m1} \\ -\eta_{12} & \eta_{22} & \cdots & -\eta_{m2} \\ \vdots & \vdots & \ddots & \vdots \\ -\eta_{1m} & -\eta_{2m} & \cdots & \eta_{mm} \end{bmatrix} \begin{bmatrix} E_1 \\ E_2 \\ \vdots \\ E_m \end{bmatrix} = \begin{bmatrix} P_1 \\ P_2 \\ \vdots \\ P_m \end{bmatrix} \tag{15}$$

This formula is the power flow balance equations of the statistical energy analysis method. The power flow balance equations include the basic parameters of statistical energy analysis (i.e., modal density, internal loss factor, coupling loss factor) and external input power.

The average sound pressure level of the acoustic subsystem j in the analysis frequency band can be calculated by the following formula:

$$SPL_{E_j} = 10\lg \frac{\rho_0 c^2 E_j}{p_r^2 V} \tag{16}$$

where p_r is the reference sound pressure, $p_r = 2 \times 10^{-5}$ Pa, and V is the volume of the acoustic space.

3.2. Numerical Model

When establishing the statistical energy analysis model of the interior aerodynamic noise of the high-speed maglev train, the following problems should be paid attention to:

(1) The modal number in the bandwidth of each subsystem with the frequency above 200 Hz should be greater than 1. However, the modal number of some subsystems with small size cannot meet this requirement, and the influence on the overall results can be ignored.

(2) Considering the size of the train body, the interior acoustic cavity is divided into three layers from top to bottom and three layers from left to right. Such division is convenient to simulate the energy transmission around the train, which can also improve the computation accuracy of the sound pressure of the receiving point at the height of 1.5 m above the floor.

(3) In order to better simulate the sound absorption inside the surface structure of the train, a thin acoustic cavity is divided close to the train surface, and the internal loss factor is computed with detailed surface parameters.

The statistical energy analysis model of the high-speed maglev train established in the present paper includes 493 subsystems—the number of car-body structure subsystems is 322 and the number of interior acoustic cavity subsystems is 171. Figure 7 shows the subsystems of the statistical energy analysis model of the high-speed maglev train.

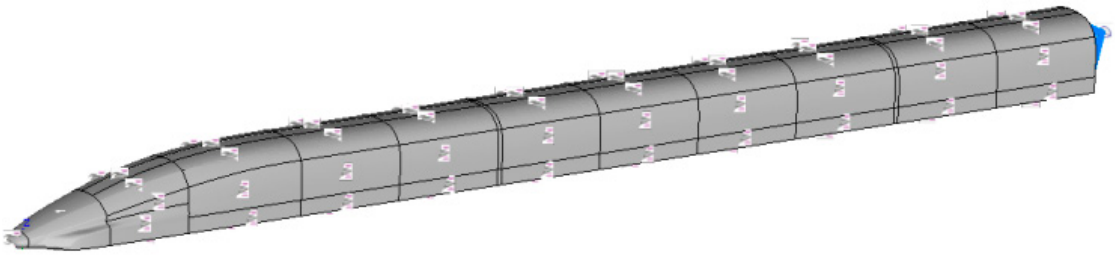

(**a**)

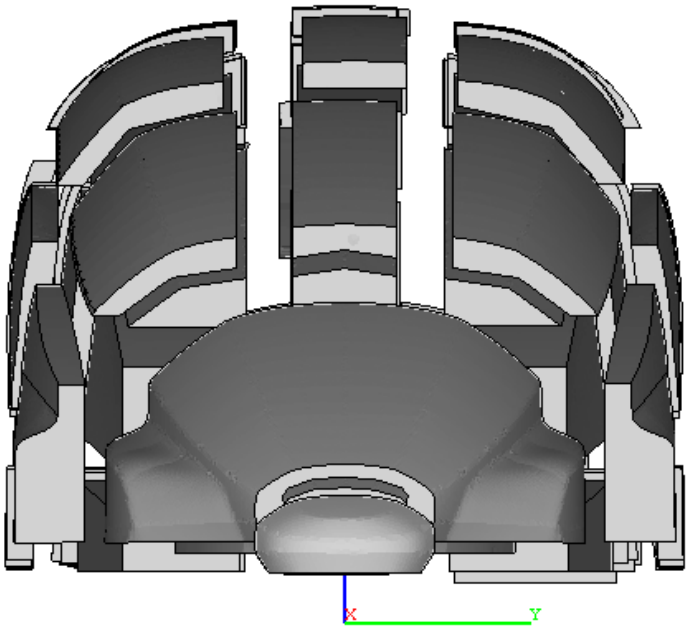

(**b**)

Figure 7. Statistical energy analysis model of the high-speed maglev train: (**a**) Side view of the subsystem division, (**b**) front view of the subsystem division.

4. Computational Results Analysis

For numerical computation, the running speed of the high-speed maglev train is 600 km/h, the tube pressure is 0.3 atm, and the tube area is 80 m^2.

Figure 8 shows the sound pressure of the interior acoustic cavity of the head and middle car with frequencies of 100 Hz, 500 Hz, 1000 Hz, and 2000 Hz. Figure 9 shows the sound pressure of the interior acoustic cavity of the tail car with frequencies of 100 Hz, 500 Hz, 1000 Hz, and 2000 Hz. It can be seen from Figures 8 and 9 that, in the low vacuum tube, distribution of the interior aerodynamic noise of the high-speed maglev train is characterized by large head/tail cars and small middle car. The interior aerodynamic noise at the top of the train is less than that at the bottom of the train. The interior aerodynamic noise of the tail car is greater than that of the head car. Meanwhile, the interior aerodynamic noise of the acoustic cavity subsystems near the floor on both sides of the train is significantly greater than that of other parts of the same cross section, which can be considered as the key parts of the interior aerodynamic noise optimization of the train.

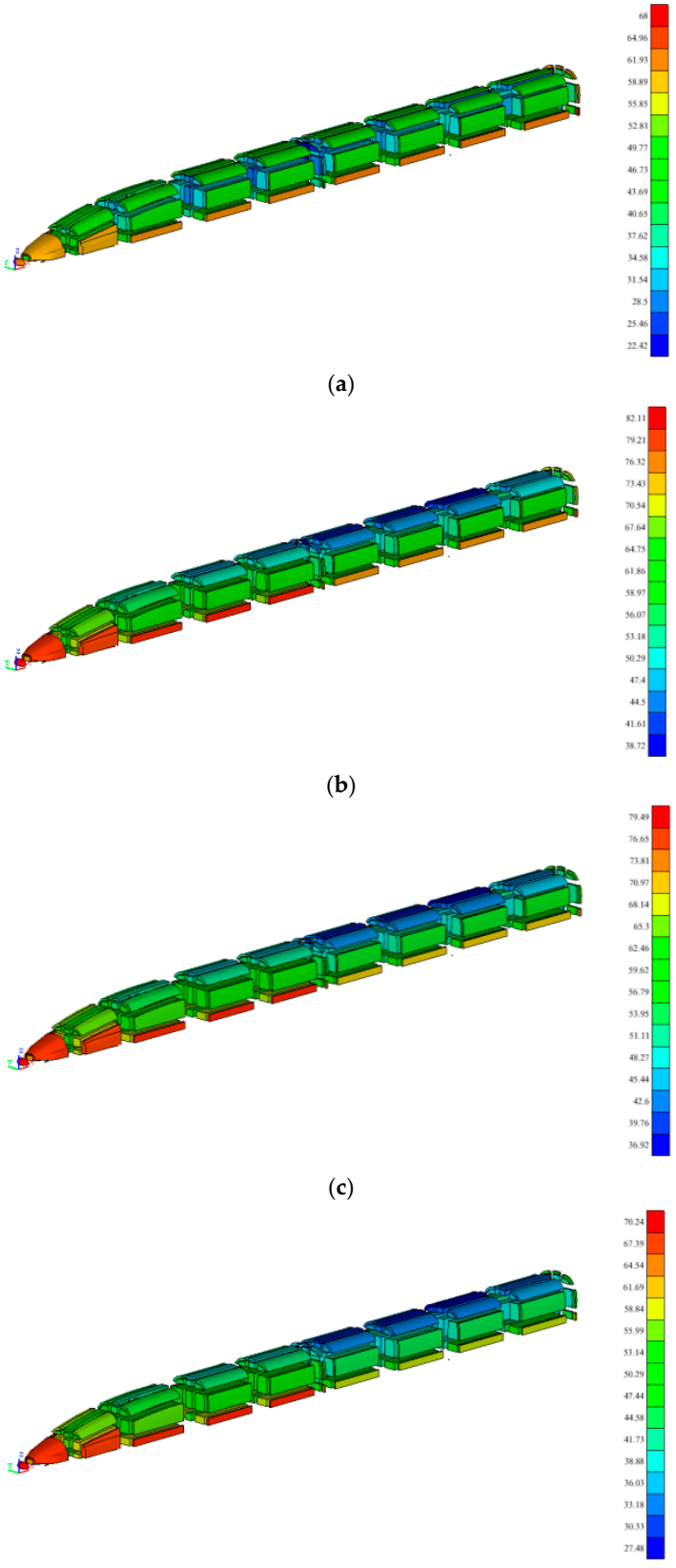

Figure 8. Interior aerodynamic noise of head and middle cars: (**a**) 100 Hz, (**b**) 500 Hz, (**c**) 1000 Hz, (**d**) 2000 Hz.

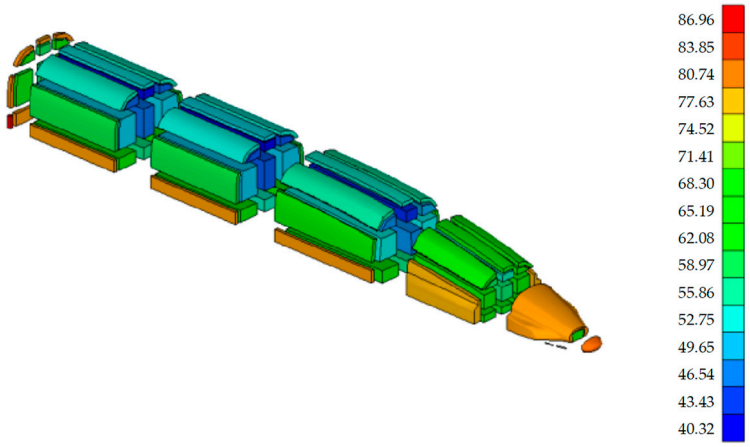

(**a**)

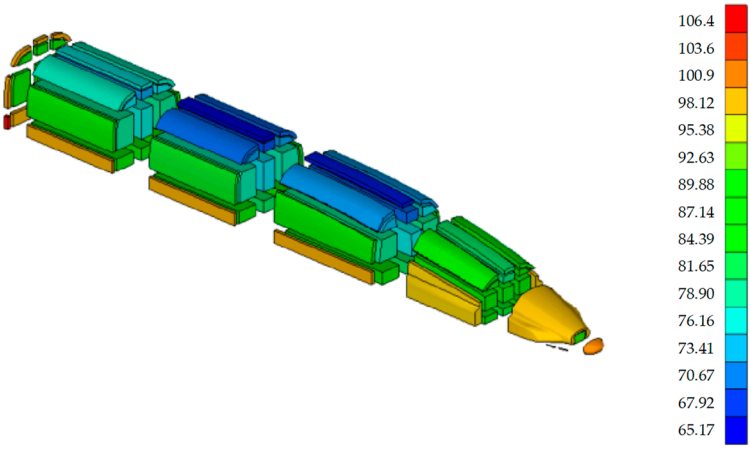

(**b**)

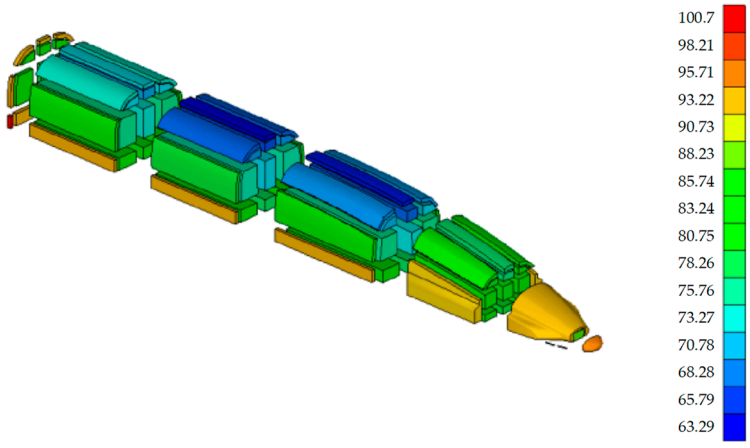

(**c**)

Figure 9. *Cont.*

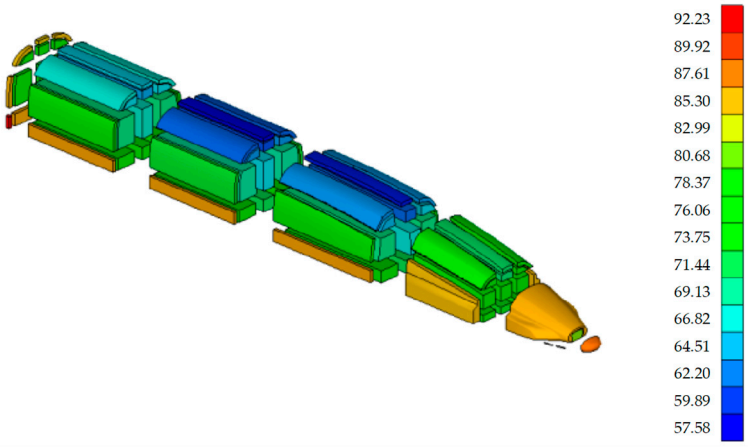

(**d**)

Figure 9. Interior aerodynamic noise of tail car: (**a**) 100 Hz, (**b**) 500 Hz, (**c**) 1000 Hz, (**d**) 2000 Hz.

The acoustic cavity subsystem in the middle of the high-speed maglev train is selected as the receiver, to study the spectrum characteristics of the interior aerodynamic noise of the high-speed maglev train. Figure 10 shows the number of the acoustic cavities in the middle of the high-speed maglev train, the number of the acoustic cavities of the head car is 1–4, the number of the acoustic cavities of the middle car is 5–8, and the number of the acoustic cavities of the tail car is 9–12.

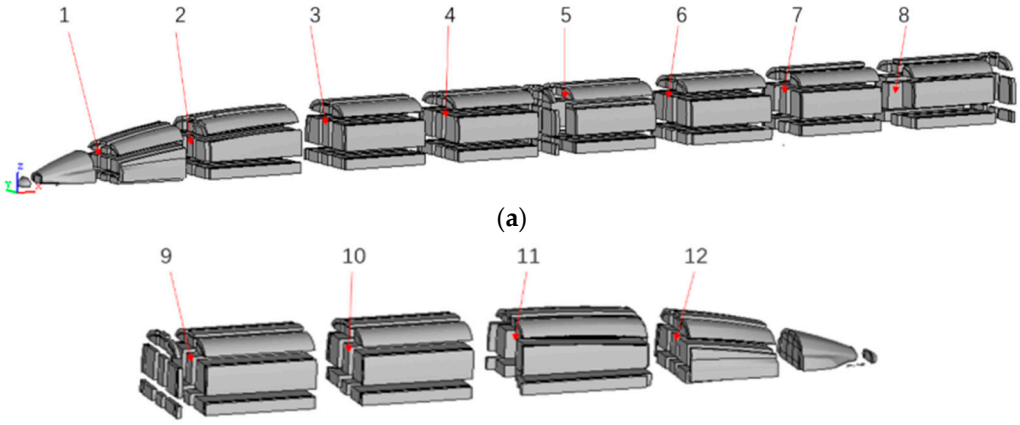

(**a**)

(**b**)

Figure 10. Number of interior acoustic cavity subsystems: (**a**) Head and middle cars, (**b**) tail car.

Figure 11 shows the sound pressure level spectrum of interior acoustic cavities 1–12 of the high-speed maglev train. It can be seen from Figure 11 that, with the increase in frequency, the sound pressure level of the interior aerodynamic noise of the high-speed maglev train has the tendency of first increasing and then decreasing, and the main energy of the interior aerodynamic noise of the high-speed maglev train in the low vacuum tube is concentrated in the range of 200–1000 Hz.

Figure 12 shows the sound pressure level totals of acoustic cavities 1–12 of the high-speed maglev train. It can be seen from Figure 12 that, the interior aerodynamic noise of the acoustic cavity subsystems of the tail car is the greatest, followed by the head car, while the interior aerodynamic noise of the acoustic cavity subsystems of the middle car is the smallest. However, in actual everyday operation as a shuttle, the direction of travel of the maglev train will change, and a tail car then becomes a head car. Therefore, both the head and tail cars should be paid special attention for the optimization of the interior aerodynamic noise.

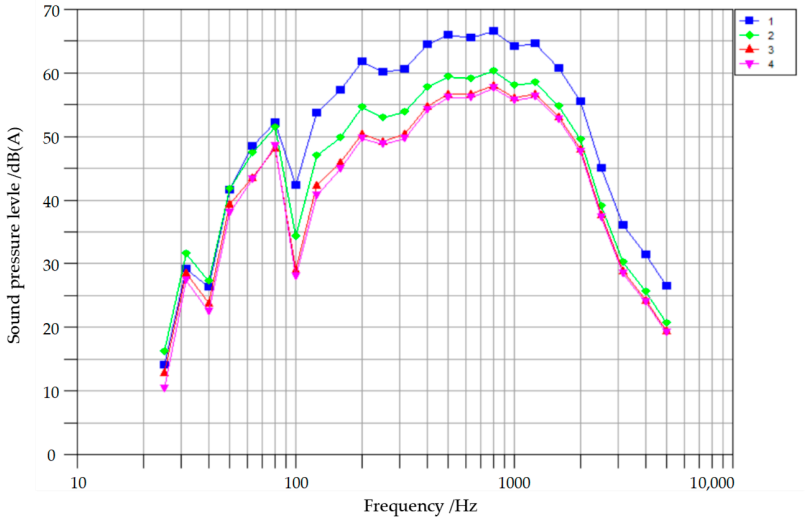

(**a**)

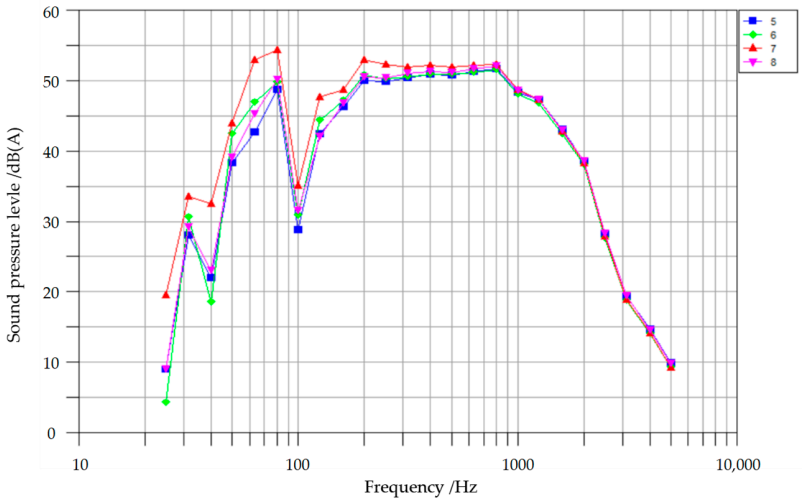

(**b**)

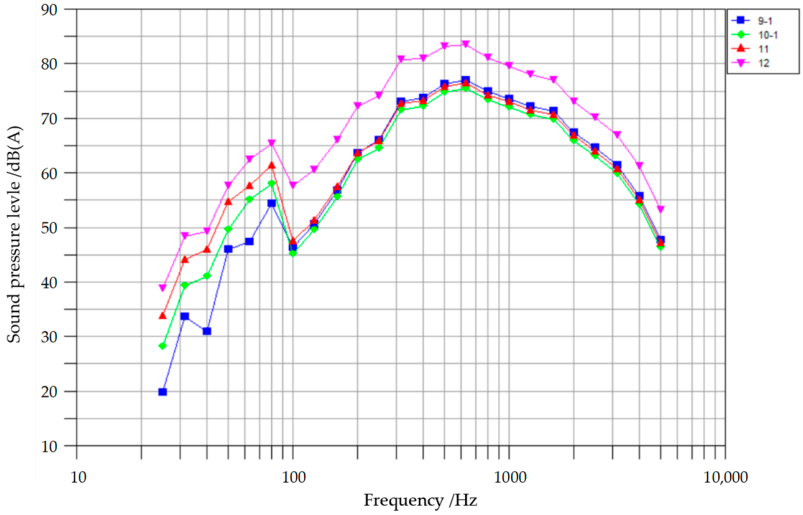

(**c**)

Figure 11. Spectrum of interior aerodynamic noise: (**a**) Spectrum characteristics of the head car, (**b**) spectrum characteristics of the middle car, (**c**) spectrum characteristics of the tail car.

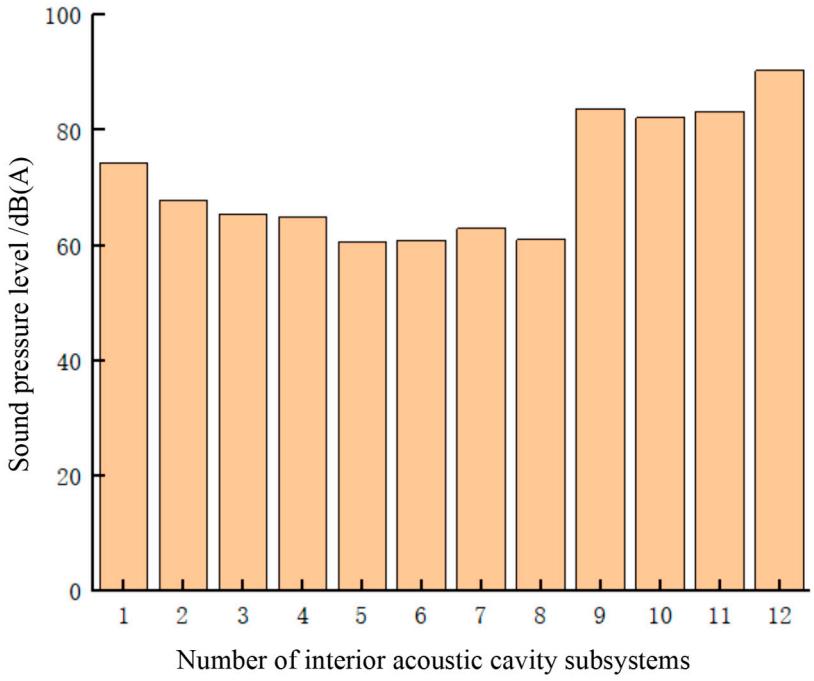

Figure 12. Sound pressure level of interior aerodynamic noise.

5. Conclusions

In the present paper, the computational models of the external flow field and interior aerodynamic noise of the high-speed maglev train in low vacuum tube were established, and the characteristics of the interior aerodynamic noise of the high-speed maglev train in the low vacuum tube were studied. The main conclusions are as follows:

(1) When the tube pressure is 0.3 atm, the air flow in the low vacuum tube is in the continuous field, and the continuous medium model can be used to describe the flow characteristics of the air in the low vacuum tube.

(2) In the vacuum tube, the distribution of the interior aerodynamic noise of the high-speed maglev train is characterized by the large head/tail cars and small middle car. The interior aerodynamic noise of the acoustic cavity subsystems near the floor on both sides of the train is significantly greater than that of other parts of the same cross section, which can be considered as the key parts of the interior aerodynamic noise optimization of the train.

(3) With the increase in frequency, the sound pressure level of the interior aerodynamic noise of the high-speed maglev train has the tendency of first increasing and then decreasing, and the main energy of the interior aerodynamic noise is concentrated in the range of 200–1000 Hz.

(4) The interior aerodynamic noise of the acoustic cavity subsystems of the tail car is the greatest, followed by the head car, while the interior aerodynamic noise of the acoustic cavity subsystems of the middle car is the smallest. As the direction of travel of the maglev train will change, the head and tail cars should be paid special attention for the optimization design of the interior aerodynamic noise.

Author Contributions: Conceptualization, J.L.; methodology, M.Y.; software, Z.Y.; validation, D.C.; formal analysis, J.L.; investigation, M.Y.; resources, D.C.; data curation, Z.Y.; writing—original draft preparation, J.L.; writing—review and editing, M.Y.; visualization, M.Y.; supervision, D.C.; project administration, Z.Y.; funding acquisition, D.C. and M.Y. All authors have read and agreed to the published version of the manuscript.

Funding: This research was funded by the Key R&D Program of Shandong Province of China (Major Scientific and Technological Innovation Project) (grant No. 2020CXGC010202), the Science and tech-

nology R & D plan of CRRC (grant No. 2020CYB110, 2022CYB199), the Natural Science Foundation of Shandong Province (Grant No. ZR2022ME180), the National Natural Science Foundation of China (grant No. 51705267), and the Postdoctoral Research Foundation of China (grant No. 2018M630750).

Institutional Review Board Statement: Not applicable.

Informed Consent Statement: Not applicable.

Conflicts of Interest: The authors declare no conflict of interest.

References

1. Ding, S.S.; Li, Q.; Tian, A.Q.; Du, J.; Liu, J.L. Aerodynamic design on high-speed trains. *Acta Mech. Sin.* **2016**, *32*, 215–232. [CrossRef]
2. Yu, M.G.; Jiang, R.C.; Zhang, Q.; Zhang, J.Y. Crosswind stability evaluation of high-speed train using different wind models. *Chin. J. Mech. Eng.* **2019**, *32*, 40. [CrossRef]
3. Li, T.; Dai, Z.Y.; Yu, M.G.; Zhang, W.H. Numerical investigation on the aerodynamic resistances of double-unit trains with different gap lengths. *Eng. Appl. Comput. Fluid Mech.* **2021**, *15*, 549–560. [CrossRef]
4. Yu, M.G.; Liu, J.L.; Dai, Z.Y. Aerodynamic characteristics of a high-speed train exposed to heavy rain environment based on non-spherical raindrop. *J. Wind Eng. Ind. Aerodyn.* **2019**, *32*, 40. [CrossRef]
5. Tan, X.M.; Wang, T.T.; Qian, B.S.; Qin, B.; Lu, Y.B. Aerodynamic noise simulation and quadrupole noise problem of 600km/h high-speed train. *IEEE Access* **2019**, *7*, 2939023. [CrossRef]
6. Thompson, D.J.; Iglesias, E.L.; Liu, X.W.; Zhu, J.Y.; Hu, Z.W. Recent developments in the prediction and control of aerodynamic noise from high-speed trains. *Int. J. Rail Transp.* **2015**, *3*, 119–150. [CrossRef]
7. Deng, Z.G.; Zhang, W.H.; Zheng, J.; Ren, Y.; Jiang, D.H.; Zheng, X.X.; Zhang, J.H.; Gao, P.F.; Lin, Q.X.; Song, B.; et al. A high temperature superconducting maglev ring test line developed in Chengdu, China. *IEEE Trans. Appl. Supercond.* **2016**, *26*, 3602408. [CrossRef]
8. Deng, Z.G.; Zhang, W.H.; Zheng, J.; Ren, Y.; Jiang, D.H.; Zheng, X.X.; Zhang, J.H.; Gao, P.F.; Lin, Q.X.; Song, B.; et al. A high-temperature superconducting maglev-evacuated tube transport (HTS Maglev-ETT) test system. *IEEE Trans. Appl. Supercond.* **2017**, *27*, 3602008. [CrossRef]
9. Kim, T.K.; Kim, K.H.; Kwon, H.B. Aerodynamic characteristic of a tube train. *J. Wind Eng. Ind. Aerodyn.* **2011**, *99*, 1187–1196. [CrossRef]
10. Oh, J.S.; Kang, T.; Hams, S.; Lee, K.; Jang, K.; Ryou, H.; Ryu, J. Numerical analysis of aerodynamic characteristics of Hyperloop system. *Energies* **2019**, *12*, 518. [CrossRef]
11. Braun, J.; Sousa, J.; Pekardan, C. Aerodynamic design and analysis of the Hyperloop. *AIAA J.* **2017**, *55*, 4053–4060. [CrossRef]
12. Opgenoord, M.M.J.; Caplan, P.C. Aerodynamic design of the Hyperloop concept. *AIAA J.* **2018**, *56*, 4261–4270. [CrossRef]
13. Niu, J.Q.; Sui, Y.; Yu, Q.J.; Cao, X.L.; Yuan, Y.P. Numerical study on the impact of Mach number on the coupling effect of aerodynamic heating and aerodynamic pressure caused by tube train. *J. Wind Eng. Ind. Aerodyn.* **2019**, *190*, 100–111. [CrossRef]
14. Niu, J.Q.; Sui, Y.; Yu, Q.J.; Cao, X.L.; Yuan, Y.P.; Yang, X.F. Effect of acceleration and deceleration of a capsule train running at transonic speed on the flow and heat transfer in the tube. *Aerosp. Sci. Technol.* **2020**, *105*, 105977.
15. Zhou, P.; Zhang, J.Y.; Li, T.; Zhang, W.H. Numerical study on wave phenomena produced by the super high-speed evacuated tube maglev train. *J. Wind Eng. Ind. Aerodyn.* **2019**, *190*, 61–70. [CrossRef]
16. Sui, Y.; Niu, J.Q.; Ricco, P.; Yuan, Y.P.; Yu, Q.J.; Cao, X.; Yang, X.F. Impact of vacuum degree on the aerodynamics of a high-speed train capsule running in a tube. *Int. J. Heat Fluid Flow* **2021**, *88*, 108752. [CrossRef]
17. Yang, Y.; Zhang, H.D.; Hong, Z.D. Research on optimal design method for drag reduction of vacuum pipeline vehicle body. *Int. J. Comput. Fluid Dyn.* **2019**, *33*, 77–86. [CrossRef]
18. Zhang, X.H.; Jiang, Y.; Li, T. Effect of Streamlined nose length on the aerodynamic performance of a 800 km/h Evacuated Tube Train. *Fluid Dyn. Mater. Process.* **2020**, *16*, 67–76. [CrossRef]
19. Nick, N.; Sato, Y. Computational fluid dynamics simulation of Hyperloop pod predicting laminar-turbulent transition. *Railw. Eng. Sci.* **2020**, *28*, 97–111. [CrossRef]
20. Klühspies, J.; Hänel, S.; Kircher, R. *Hyperloop? Results of an International Survey in the Transport Sector*; The International Maglev Board: Munich, Germany, 2022.
21. He, K.; Su, X.C.; Gao, G.J.; Krajnović, S. Evaluation of LES, IDDES and URANS for prediction of flow around a streamlined high-speed train. *J. Wind Eng. Ind. Aerodyn.* **2022**, *223*, 104952. [CrossRef]
22. Li, T.; Qin, D.; Zhang, W.H.; Zhang, J.Y. Study on the aerodynamic noise characteristics of high-speed pantographs with different strip spacings. *J. Wind. Eng. Ind. Aerodyn.* **2020**, *202*, 104191. [CrossRef]
23. Chen, Q.; Fei, Q.G.; Wu, S.Q.; Li, Y.B. Statistical energy analysis for the vibro-acoustic system with interval parameters. *J. Aircr.* **2019**, *56*, 1869–1879. [CrossRef]
24. Lee, H.R.; Kim, H.Y.; Jeon, J.H.; Kang, Y.J. Application of global sensitivity analysis to statistical energy analysis: Vehicle model development and transmission path contribution. *Appl. Acoust.* **2019**, *146*, 368–389. [CrossRef]